Completely decentralised active balancing battery management system

Damien F. Frost, *Student Member, IEEE,* and David A. Howey, *Member, IEEE*

***Abstract*—The performance of a string of series-connected batteries is typically restricted by the worst cell in the string and a single failure point will render the entire string unusable. To address these issues, we present a decentralised battery management system with no communication requirement based on a modular multilevel converter topology with a distributed inductor and distributed controller running on a local microprocessor. This configuration is referred to as a "smart cell". By sensing the voltage across the local distributed inductor, each smart cell is able to (1) determine its optimal switching pattern in order to minimize the output voltage ripple, and (2) adjust its duty cycle to synchronize its state of charge with the average state of charge of the series string of cells. The decentralized controller is derived using the theory of Kuramoto oscillators, and the stability of a system of smart cells is investigated. We show experimentally that a system of three smart cells with their decentralized controllers can accurately synchronize the state of charge while minimizing their output voltage ripple.**

I. Introduction

THE integration of power electronics into the interfaces of green energy technologies to the grid is playing a key role in the reduction of greenhouse gas emissions [1], [2]. In particular, electrical energy storage systems such as lithium-ion battery packs are seeing an increased penetration of power electronics [3], and the market for such devices is growing very rapidly as costs decrease [4]. Grid connected energy storage systems require state of the art power electronics converters and energy management systems to ensure that the most expensive component of the energy storage system, the electrochemical battery pack [5], is operated in a safe and reliable manner [6], [7].

Alongside this, many companies who sell electric vehicles (EVs) and hybrid electric vehicles (HEVs) are investigating innovative ways to handle the influx of battery waste from these vehicles. The battery of an EV or HEV is considered to be at the end of its (first) life if its state of health (SOH), usually measured in terms of nominal capacity, falls to around 70%-80% of its original value [8], [9]. Although at this point the battery pack may be considered useless for portable applications, it still contains a lot of residual value for stationary energy storage applications [10], [11]. Recently, there have been announcements from Nissan [12], BMW [13], and GM [14], who are all experimenting with energy storage systems using batteries recovered from their EVs and HEVs.

For certain cell chemistries, individual cell monitoring is necessary. As an example, lithium-ion battery technology is unsafe if overcharged, where cells may explode or rupture [15], [16]. In the worst case scenario, an unmanaged series string of batteries will be limited by the weakest cell [17], thus a single failed cell can render the entire string useless. Therefore, in order to maximize the energy storage potential of several cells connected together in a pack, especially cells of varying capacities and usage histories, the state of charge of individual cells in a battery pack must be measured and balanced. For enhanced performance, active cell balancing is chosen as the preferred method. Active cell balancing circuits fall within two main categories: energy re-allocation and variable loading/charging. The most basic energy re-allocation topology uses a switched capacitor system [18], [19], [20], however since the amount of charge moved from one cell to another is proportional to the difference in cell voltage, balancing times are slow especially as the cells become more balanced. In order to overcome some of the drawbacks of switched capacitor topologies, balancing circuits using a multi-winding flyback topology have also been proposed[21], [22]. In general, all energy re-allocation topologies are only able to cope with a small mismatch is cell capacities, and therefore are not suitable in situations where cells have wildly varying capacities.

The drawbacks of balancing with energy re-allocation can be overcome with active balancing by variable loading/charging. This can be accomplished by placing an individual power converter and battery management system on every cell [23], [24], [25]. Although active cell management at the cell level is still an expensive option, recent advancements in wide band gap switching devices, whose cost is expected to decrease over time, will increase conversion efficiencies (and reduce power losses), and reduce overall system costs through higher power density [26], [27], [28] and decreased cooling requirements [29].

We present work on a cell level battery management system (BMS) and power converter which uses a decentralized control strategy to regulate the state of charge of serially connected cells of varying capacities. In the literature there are examples of battery management systems with global information and control [30], [31], [32], systems with low bandwidth communication [33], [34], or a sparse communication networks [35], [36], [35], and systems that use isolated cell level converters connected to an auxiliary voltage bus implementing a droop controller [37], [38]. Conversely, this work introduces a completely decentralized controller that *does not rely on any communication, or an auxiliary voltage bus*. The distributed battery management system is designed to discharge and charge each cell in a series string of cells proportional to its

D. F. Frost and D. A. Howey are with the Department of Engineering Science, University of Oxford, Oxford, OX1 3PJ, United Kingdom

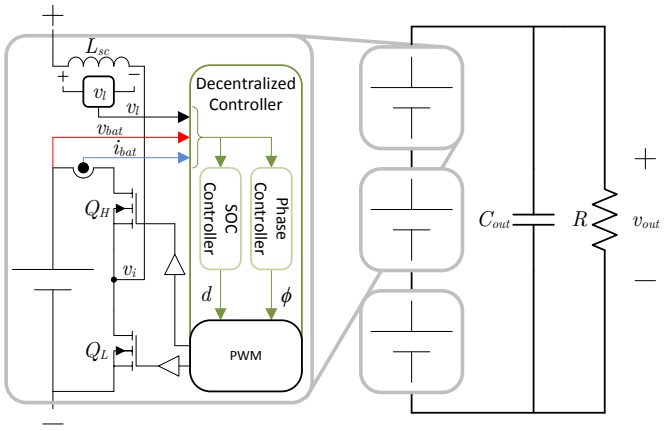


Fig. 1: An example of a system containing three 'smart cells'.

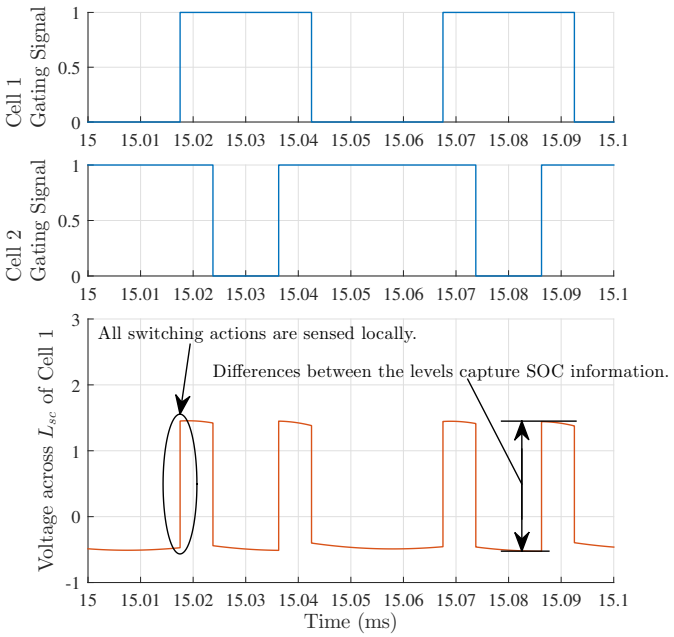


Fig. 2: A simulation of two smart cells switching, showing the voltage across the sensing inductor and its salient features.

capacity using a local converter that can actively balance its local cell with variable loading/charging. The converters are also controlled in such a way as to minimize the size of the filtering components in the series string.

II. System Architecture

An example of the proposed system architecture is shown in Fig. 1, and was first presented by the authors in [39]. In this example, the system is constructed out of three MMC cells each containing a half bridge switching network similar to the switching networks found in the sub-modules of MMC converters [40]. The MMC topology has already been used to integrate large battery packs for high power applications [32], [41], however what we are proposing is to use the MMC in a low power application. Each submodule, which we shall in this paper call a 'smart cell', has two distinct features that make it different from a standard MMC submodule:

1) There exists an independent, decentralized controller in each smart cell.
2) Each smart cell includes a small filter inductor, L_{sc}.

The decentralized controller manages the state of charge (SOC), and monitors the state of health (SOH) of its locally connected battery cell. This information is used to apply a duty cycle to the switches Q_L and Q_H, such that the connected battery cell discharges in proportion to its capacity. Discharging all cells in proportion to their respective capacities yields two large benefits for the string of smart cells:

1) The SOC of all of the cells in the string will be synchronized.
2) Larger, healthier battery cells will be loaded more than the smaller, more degraded battery cells, thus the pack will degrade at a more uniform rate [42].

The voltage across the small filter inductor, v_l, contains all of the information required for each smart cell to determine its optimal switching pattern, and to adjust its duty cycle to synchronize its SOC with the other smart cells in the string. Fig. 2 is a simulation of a two smart cell system switching in its optimal switching pattern, with the voltage across one of the sense inductors shown. As shown in the figure, all of the switching transitions are captured by the sense inductor, L_{sc}. Section III describes how the optimal switching pattern is obtained using the transitions of v_l, and Section IV describes how the phase controller of Fig. 1 is designed. Section VI describes how the SOC of the string is synchronized using the voltage across v_l, and the design of the SOC controller of Fig. 1.

In addition to sensing, L_{sc} is used as a distributed inductor to provide output filtering. Eventually L_{sc} could be small enough to be implemented on the trace of a PCB, greatly reducing the cost and size of this component. The dc output to the load requires a small filter capacitor, C_{out}, whose capacitance depends on the application requirements.

III. Optimal Switching Pattern

In order to minimize the output voltage ripple measured at v_{out} an optimal switching pattern of all of the switches Q_H and Q_L, of all of the smart cells, must be determined. This is done by all smart cells collectively minimizing the ac rms inductor current. The full derivations of the results of this section were originally presented in [39].

Given a set of M battery cells with capacities $\boldsymbol{C} = \{C_1, C_2, \ldots, C_M\}$, our objective is to find a set of phase timings, $\boldsymbol{\theta} = \{\theta_1, \theta_2, \ldots, \theta_M\}$ for the turn-on of each smart cell which will minimize the ripple current in the local inductor L_{sc}, thus minimizing the output ripple voltage. It is reasonable to assume that the nominal voltage of all of the battery cells is $V_{nom} = V_1 = V_2 = \ldots = V_M$, since the SOC of all of the battery cells will be synchronized. The duty cycle of the ith smart cell can be calculated using the following equation:

$$D_i = \frac{C_i}{C_{MAX}} \tag{1}$$

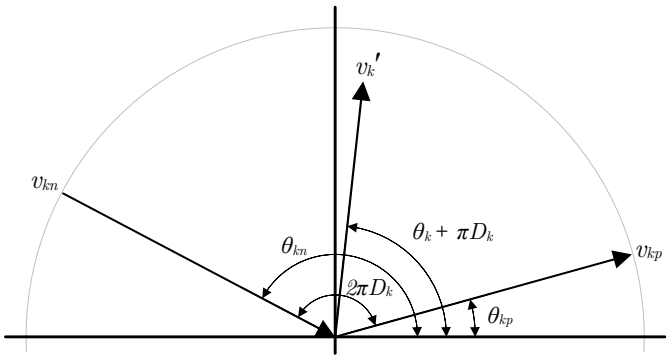


Fig. 3: Representing the switching action of the k^{th} smart cell as a vector, with its weighted, phase shifted vector, v'_k. The switching actions of the k^{th} smart cell are also shown as vectors v_{kp} and v_{kn}.

where C_{MAX} is the maximum capacity expected within set $\boldsymbol{C}$ amongst all of the cells, such that $0 \leq D_i \leq 1$ for all i. In [39], the authors show that an analytical expression for the ac rms inductor current as a function of the smart cells' duty cycles and phase angles is:

$$I^2_{Lac-rms} = \frac{1}{2}\left(\frac{V_{nom}T_s}{2\pi L}\right)^2 \sum_{n=1}^{\infty}\sum_{i=1}^{M}\sum_{j=1}^{M}\frac{4}{\pi^2 n^4}\cdot$$
$$[\sin(\pi n D_i)\ \sin(\pi n D_j)\cos(\pi n(D_i - D_j) + n(\theta_i - \theta_j))] \quad (2)$$

Equation (2) can be minimized to determine an optimal set $\boldsymbol{\theta} = \{\theta_1, \theta_2, \ldots, \theta_M\}$ that will minimize the ac rms current in the inductor L_{sc}, and therefore, the output voltage ripple in v_{out}.

A. Simplifying the problem

Examining (2), we see that solving for an optimal set $\boldsymbol{\theta}$ to minimize $I_{Lac-rms}$ is non trivial, and difficult to achieve without significant computational power and global information about the system. Therefore in this section we present a way to identify a set $\boldsymbol{\theta}$ which will yield a satisfactory solution, with significantly less computational requirements, and in a decentralized fashion.

First, let us represent the switching action of the k^{th} smart cell as a vector, v_k, in the unit circle as depicted in Fig. 3. The k^{th} smart cell will turn on at θ_k, and turn off at $\theta_k + 2\pi D_k$. Now define a new vector, v'_k which will be known as the weighted vector, whose phase places the vector half way between the turn on and turn off times and whose length is $\sin(\pi D_k)$. Therefore the phase and length of the weighted vector, v'_k, are given by:

$$\angle v'_k = \theta'_k = \theta_k + \pi D_k \quad (3)$$
$$|v'_k| = \sin(\pi D_k) \quad (4)$$

Applying the transformation described in (3) and (4) to all of the smart cells, and summing all v'_k, we can find the square of the magnitude of the total sum vector, $|v'_\Sigma|^2$:

$$|v'_\Sigma|^2 = \sum_{i=1}^{M}\sum_{j=1}^{M}\sin(\pi D_i)\sin(\pi D_j)\cos(\pi(D_i - D_j) + \theta_i - \theta_j) \quad (5)$$

Equation (5) has the exact same form as (2) when $n = 1$ (i.e. only the fundamental is considered). Therefore, one control algorithm that will yield a sub-optimal but acceptable minimum of (2) is to minimize the magnitude of the total sum vector, $|v'_\Sigma|^2$.

B. Extracting information from v_l

In order to minimize the magnitude of the total sum vector, $|v'_\Sigma|^2$, found in (5), the duty cycle and phase shift of every smart cell in the string is still required. As shown in Fig. 2, every time a smart cell switches in and out of the string, this transition is captured by every sense inductor, L_{sc}, in the string of smart cells. Therefore, by observing when all of the positive and negative transitions occur in v_l, the "on" and "off" times of all of the smart cells in the string can be determined. From this information, the phase shift and "on" times of each cell in the string can be determined. The corresponding "off" time, and therefore duty cycle of each cell, cannot be uniquely determined.

However, as the authors have shown in [39], there is no need to *pair* the correct "off" transition to its "on" transition in order to minimize (5). Even if "on" and "off" transitions are incorrectly paired together, the same minimum of (5) will be found.

IV. Phase Controller Design

The smart cell controller needs to be designed such that a group of cells working together will minimize (5). By taking the derivative of (5) and setting it to zero, the local minima can be found. The partial derivative of (5) with respect to θ_k is shown below:

$$\frac{\partial |v'_\Sigma|^2}{\partial \theta_k} = 2\sin(\pi D_k)\sum_{i=1;i\neq k}^{M}\sin(\pi D_i)\sin(\pi(D_i - D_k) + \theta_i - \theta_k) \quad (6)$$

Graphically, setting (6) to zero is equivalent to "pointing" the weighted vector v'_k in either 1) an opposite direction, or 2) the same direction, to all of the other weighted vectors $v'_{i,i\neq k}$ summed together. Clearly, by "pointing" v'_k in the same direction as $\sum_i v'_{i,i\neq k}$ would result in large currents in the inductor since all of the cells would eventually be in phase, maximizing the ripple current. However, if we chose to direct v'_k in the *opposite* direction to $\sum_i v'_{i,i\neq k}$, the current through the inductors will be reduced. Fig. 4 summarizes this observation.

Therefore, during each iteration of the smart cell controller, every smart cell will sum up the weighted vectors of all of the other smart cells it senses, and set its local reference to be 180 degrees away from that sum. By doing this, each smart cell will be driving (6) to zero, thus finding a local minimum to (5). Using this controller design, (7) defines the reference angle, $\theta'_{k,ref}$, for the kth smart cell's weighted sum vector, v'_k.

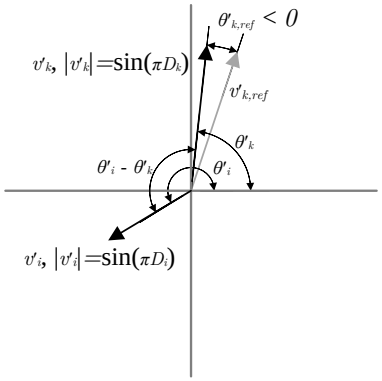


Fig. 4: Graphical representation of the weighted vectors v'_k and v'_i. By pointing these two vectors in the opposite direction, (5) will be minimized. This is accomplished with the controller of (7).

$$\theta'_{k,ref} = -2\sin(\pi D_k)\sum_{i=1;i\neq k}^{M}\sin(\pi D_i)\sin(\pi(D_i-D_k)+\theta_i-\theta_k) \tag{7}$$

Note the negative sign in (7), this ensures that that the angle between $\theta'_{k,ref}$ and $\sum_i v'_{i,i\neq k}$ is driven to π. Using (7) and the angle transformation of (3), a non-linear model for the k^{th} smart cell controller can be constructed, and is shown below:

$$\dot{\theta}'_k = \omega_k - 2\frac{K}{M}\sin(\pi D_k)\sum_{i=1;i\neq k}^{M}\sin(\pi D_i)\sin\left(\theta'_i-\theta'_k\right) \tag{8}$$

where ω_k is the switching frequency, and K is a controller constant.

V. Phase Controller Stability Analysis

Using the smart cell controller model developed in Section IV, the stability of a group of smart cells around local minima of (6) will be investigated. First note that the controller chosen in (8) is very similar to the Kuramoto model of coupled oscillators [43], which is repeated in (9)

$$\dot{\theta}_k = \omega + \frac{K}{M}\sum_{i=1}^{N}\sin(\theta_i-\theta_k), \tag{9}$$

where ω is the nominal switching frequency of the system, M is the number of agents, and K is a global controller constant, identical for all agents.

First, consider the dynamics of the system described by (8) in a rotating reference frame, where all of the ω_k's are equal, thus $\omega_k = \omega$, and let

$$\theta'_k = \omega t + \gamma'_k. \tag{10}$$

Equation (8) becomes:

$$\dot{\gamma}'_k = -2\frac{K}{M}\sin(\pi D_k)\sum_{i=1;i\neq k}^{M}\sin(\pi D_i)\sin\left(\gamma'_i-\gamma'_k\right) = f_k\left(\boldsymbol{\Gamma'}\right) \tag{11}$$

where $\boldsymbol{\Gamma'} = \{\gamma'_1, \gamma'_2, \ldots \gamma'_M\}$. Linearize (11) around the equilibrium point $\boldsymbol{\Gamma'^{\star}} = \{\gamma^{\star}_1, \gamma^{\star}_2, \ldots \gamma^{\star}_M\}$, to create the linear system defined by (12), which will be used to assess the stability of a group of smart cells around local minima of (5).

$$\dot{\boldsymbol{\Gamma}}' = -\frac{K}{M}\boldsymbol{L}\cdot\boldsymbol{\Gamma'} \tag{12}$$

where $\boldsymbol{L}$ is equivalent to the Jacobian matrix of (11) evaluated at the equilibrium point $\boldsymbol{\Gamma'^{\star}}$. Therefore, each element, L_{ij}, of the matrix $\boldsymbol{L}$ is defined explicitly as:

$$L_{ij} = \begin{cases} -2\sin(\pi D_j)\sum_{i=1;i\neq j}^{M}\sin(\pi D_i)\cos\left(\gamma^{\star}_i-\gamma^{\star}_j\right), & i=j \\ 2\sin(\pi D_j)\sin(\pi D_i)\cos\left(\gamma^{\star}_i-\gamma^{\star}_j\right), & i\neq j \end{cases} \tag{13}$$

The matrix $\boldsymbol{L}$ can also be represented by the partial derivatives of (5). Letting $\Theta^{\star} = \{\theta^{\star}_1, \theta^{\star}_2, \cdots, \theta^{\star}_M\}$ be the corresponding equilibrium point of $\boldsymbol{\Gamma'^{\star}}$, yields:

$$\boldsymbol{L} = \begin{bmatrix} \left.\frac{\partial^2|v'_\Sigma|^2}{\partial\theta_1^2}\right|_{\Theta^{\star}} & \left.\frac{\partial^2|v'_\Sigma|^2}{\partial\theta_1\partial\theta_2}\right|_{\Theta^{\star}} & \cdots & \left.\frac{\partial^2|v'_\Sigma|^2}{\partial\theta_1\partial\theta_M}\right|_{\Theta^{\star}} \\ \left.\frac{\partial^2|v'_\Sigma|^2}{\partial\theta_2\partial\theta_1}\right|_{\Theta^{\star}} & \left.\frac{\partial^2|v'_\Sigma|^2}{\partial\theta_2^2}\right|_{\Theta^{\star}} & \cdots & \left.\frac{\partial^2|v'_\Sigma|^2}{\partial\theta_2\partial\theta_M}\right|_{\Theta^{\star}} \\ \vdots & \vdots & \ddots & \vdots \\ \left.\frac{\partial^2|v'_\Sigma|^2}{\partial\theta_M\partial\theta_1}\right|_{\Theta^{\star}} & \left.\frac{\partial^2|v'_\Sigma|^2}{\partial\theta_M\partial\theta_2}\right|_{\Theta^{\star}} & \cdots & \left.\frac{\partial^2|v'_\Sigma|^2}{\partial\theta_M^2}\right|_{\Theta^{\star}} \end{bmatrix} \tag{14}$$

Equation (14) is simply the Hessian of the total sum vector, $|v'_\Sigma|^2$ of (5) evaluated at $\Theta^{\star}$. Since we chose $\Theta^{\star}$ to be a local minimum of (5), we also know that (14) is positive semi-definite. Therefore, all of the eigenvalues of $-\boldsymbol{L}$ are all less than or equal to zero. As a consequence, the local minimum point, $\Theta^{\star}$, is an asymptotically attracting equilibrium point, and therefore a stable operating point.

It is not possible for $\boldsymbol{L}$ to be positive definite. This is due to the cyclic nature of oscillatory systems. For example, if $\Theta^{\star}$ is a local minimum, then so is $\Theta^{\star}+x$, where x is any angle. However, since we are only concerned about the relative angle between the smart cells to minimize (5), this is expected.

VI. SOC Controller Design

The SOC of each smart cell is regulated by synchronizing its SOC with the average SOC of a series string of smart cells, which is determined by analysing v_l, the voltage across the sense inductor, L_{sc}. The SOC controller relies on the string of smart cells being composed of cells of the same chemistry, so that there is a consistent relationship between the SOC and cell terminal voltage throughout the string.

As shown in Fig. 2, every time a smart cell switches in and out of the string, the voltage that it switches will be sensed by all of the sense inductors in the string of smart cells. Therefore, by calculating the differences in the levels of the v_l waveform, the terminal voltage of the cell that switched in or out can be extracted by each smart cell. Averaging all of these differences yields an average terminal voltage for the series string of smart cells. In order to account for variations in the inductance of L_{SC} and the sensing hardware, the gain of the v_l sensor is measured

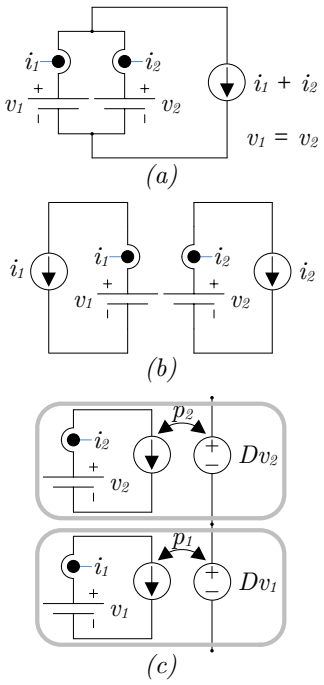


Fig. 5: Schematic showing the equivalence between the SOC controller of the smart cells and operation of the same cells in a parallel configuration.

and adjusted every time the SOC controller is executed. Since the local cell knows its duty cycle and phase, it can determine which transitions in the v_l waveform are caused by its cell switching in and out of the circuit. Using these transitions, along with the local cell voltage measurement, the local cell can calculate the gain of its v_l sensor to correctly determine the voltages of the other cells switching in and out of the circuit.

The SOC controller adjusts the duty cycle of the local cell using a simple proportional-integral (PI) controller to synchronize its terminal voltage with the string's average terminal voltage. Operation in this manner is equivalent to operating the cells in parallel, as shown in the two cell example of Fig. 5. When two cells form a parallel pack of parallel cells, their terminal voltages are equal, and their output currents are i_1 and i_2, where i_1 is not necessarily the same as i_2, as shown in Fig. 5 (a). One can split up this parallel connection, and load each cell individually with i_1 and i_2 such that their terminal voltages are *still* equal, as shown in Fig. 5 (b). Thus, the two cells are operating as if they were connected in parallel. Finally, one can place the two cells in series as shown in Fig. 5 (c), operating them with currents i_1 and i_2, such that their terminal voltages are equal, and using a power converter to enable the series connection. The SOCs of parallel connected cells are considered to be nearly identical, and require no further management [44]. Thus, the SOC of series connected smart cells will also be well synchronized, without having to directly compute their SOC.

The one difference between the series connection of cells as shown in Fig. 5 (c) and the parallel connection of cells as shown in Fig. 5 (a), is that during rest (when there is no current flowing through the cells), the cell voltages will slowly return to their true open circuit voltage. During this time, there may be current flowing between the parallel cells as each cell's internal chemical states reach their equilibrium. Although this would mean that the parallel cells would be perfectly balanced, this is not always necessarily advantageous, as there would be spurious current flowing during an 'off' state, leading to ohmic losses and heat generation in the cells.

VII. Implementation of the Control Algorithm

A MATLAB-Simulink model of a smart cell using the theory developed in this work was built using the SimPowerSystems toolbox. The model uses the Simscape battery model and MOSFETs to simulate the power circuit. The controller was implemented as an embedded MATLAB function, and is executed once per switching cycle when the upper MOSFET, Q_H, is switched on.

Fig. 6 illustrates the algorithm the controller implements as a block diagram. Steps 1 through 5 are implemented by the embedded MATLAB function.

1) **Signal Processor:** Detects all of the positive and negative transitions that occur during every switching cycle, T_s. The local cell voltage, V_{local}, and the average cell voltage, V_{avg}, are measured using the levels of the v_l waveform. The edge detector also keeps track of the number of smart cells sensed in the string with a simple low pass filter to average the number of smart cells.
2) **Calculate $\theta'_{k,ref}$:** A new reference phase shift is calculated using (7).
3) **Calculate $\theta'_{k,new}$:** The new phase that will be sent to the PWM generator is calculated by the phase controller.
4) **Apply limits:** $\pm 2\pi$ is added to $\theta'_{k,ref}$ until it lies between $-\pi$ and π.
5) **SOC Controller:** A new duty cycle is computed using V_{local} and V_{avg}. The updated duty cycle, D_k, is sent to the PWM module.
6) **PWM Generator:** $\theta'_{k,new}$ is used by the PWM generator to produce gating signals for the MOSFETs.

The phase control loop, defined by steps 1 to 4 in Fig. 6, runs a hundred times faster than the SOC control loop. The SOC control loop is defined by steps 1 and 5, and will not modify the duty cycle unless the phase controller has reached a steady state value.

The embedded MATLAB function that implements the controllers, was converted into C++ code by MATLAB's coder toolbox, for easy integration into the hardware.

VIII. Simulation Study of the Phase Controller

A simulation study of a series string of three smart cells was undertaken to investigate the stability of the phase controller. Table I lists the simulation parameters used. The controller gain, K, was chosen through experimentation.

The simulation consists of the three smart cells operating completely independently of each other. The optimal switching controller is turned on 1.0 ms into the simulation. A value of $C_{MAX} = 4.00$ Ah was pre-programmed into each smart cell,

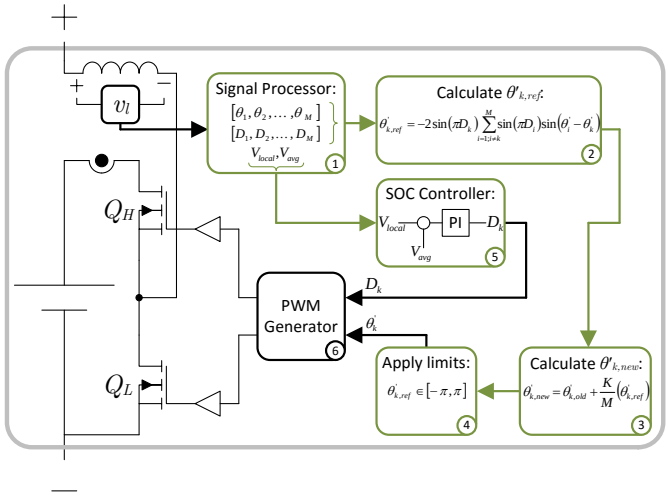


Fig. 6: Control block diagram of a smart cell built in MATLAB-Simulink. The steps 1 to 5 outlined in green, are implemented in an embedded MATLAB function.

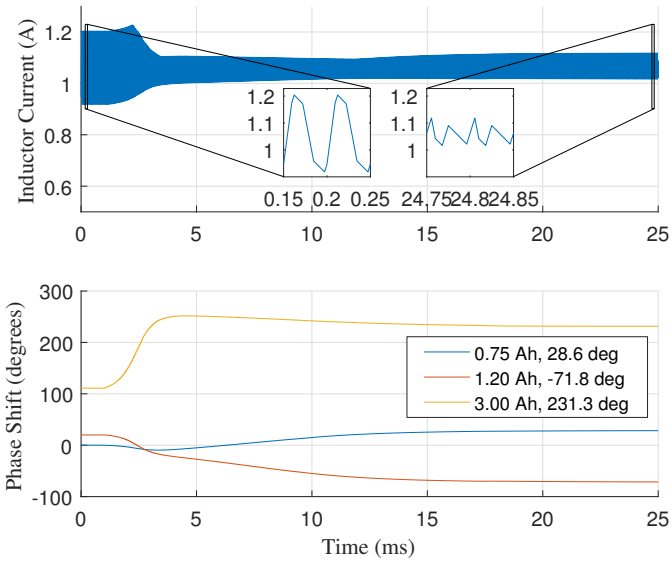


Fig. 7: Summary of the simulation results of a three smart cell pack. The smart cell controllers are turned on at 1.0 ms. The ac rms current in the inductor is improved from 103 mA rms to 26 mA rms. Although not shown, the peak-to-peak ripple voltage on the capacitor is improved from 43 mV to 6 mV.

TABLE I: Parameters of the two smart cell simulation study.

Description	Parameter	Value
Battery Cell Capacities	C_1	0.75 Ah
	C_2	1.20 Ah
	C_3	3.00 Ah
Smart Cell Parameters	L_{sc}	100 μH
	f_s	20 kHz
	V_{nom}	4.19 V
Output	C_{out}	54.7 μF
	R	4.8 Ω
Control Parameters	K	10

in order for each smart cell to calculate its local duty cycle according to (1).

Fig. 7 shows how different characteristics of the system evolve over the length of the simulation. The smart cells initially all turn on at the same time, which produces a very high ac rms ripple current in the inductor, as shown in the inset graphs. At the beginning of the simulation, $I_{Lac-rms}$ is 103 mA rms, and the peak-to-peak output voltage, v_{out-pp}, is 43 mV. After the optimal switching controller is engaged, the phase shift of each smart cell gradually evolves smoothly into its steady state value. At the end of the simulation, $I_{Lac-rms}$ and v_{out-pp} have improved considerably to 26 mA rms and 6 mV, respectively. The amount of ripple current and ripple voltage reduction will depend heavily on duty cycles of the smart cells, thus a different group of smart cells may have less or more ripple reduction than shown here.

IX. Experimental Results

A. Hardware Setup

The theory developed in this work was tested in the laboratory with an experimental setup consisting of three smart cells in series, as shown in Fig. 1 using the parameters listed in Table I. The hardware was built around ARM's *mbed* platform, where each smart cell is implemented with the NUCLEO-F401RE board and a custom printed circuit board (PCB) containing the power stage. The inputs of each smart cell PCB was connected to a small pack of parallel connected 18650 lithium-ion cells, in order to simulate battery cells of varying capacities. Table II lists the capacities of the equivalent cell connected to each smart cell, as measured by a Neware battery tester, 8 channel 5V20A-NTFA. The cells used were manufactured by Samsung, model number INR18650-29E [45]. The outputs of the smart cells were connected in series, and attached to a 4.8 Ω resistive load. Fig. 8 shows a photograph of the three smart cells built in the laboratory.

TABLE II: Cell capacities used to test three smart cell PCBs in the laboratory.

Cell	Number of 18650 Cells	Measured Capacity
1	3	7.97 Ah
2	3	8.10 Ah
3	2	5.31 Ah

The NUCLEO-F401RE board was chosen for its relatively powerful micro-controller, the STM32F401RET6, in order to focus attention on how the smart cell controller can be implemented in hardware. The STM32F401RET6 is based on the ARM 32-bit Cortex-M4 CPU and has a floating point unit. The analog to digital converter of the STM32F401RET6 was configured to its highest sample rate of 2.8 MHz while maintaining 12 bit sampling resolution, to capture the details of the v_l waveform. The sampling rate and resolution of the ADC determine the accuracy of the phase controller and SOC

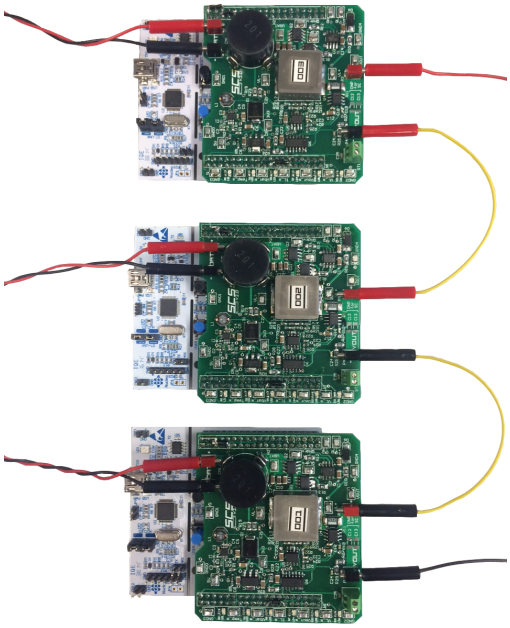


Fig. 8: A photograph of the three smart cell system operating in the laboratory. The battery cell connections are on the left, and the output is on the right. The smart cells were connected to a variety of cells.



Fig. 9: An oscilloscope screen shot of the three smart cells operating at their optimal switching pattern, averaging applied with 8 samples. Channel 2, top green trace, is the voltage across L_{sc} of the first smart cell with a capacity of C_1. Channel 2, middle blue trace, is the output voltage ripple. Channel 3, bottom pink trace, is the current in the smart cell inductors.

controller, respectively. The ADC used in these experiments was able to detect changes in phase of 2.6 degrees, and 3.6 mV change in terminal voltages. Using the same ADC, tighter phase regulation could be achieved by decreasing the switching frequency.

B. Phase Controller Performance

A first experiment using the pre-programmed capacities of Table I was carried out to verify the performance of the phase controller, whose role is to reduce the ac-rms current through the series string of smart cells.

Fig. 9 shows an oscilloscope screen shot of the four smart cells operating and finding their optimal switching pattern. The peak-to-peak voltage ripple from the experiments was reduced to 23 mV from 145 mV and the ac-rms L_{sc} ripple current was reduced to 25 mA rms from 95 mA rms. Note that the peak to peak value calculated by the oscilloscope, and shown in Fig. 9, includes some switching noise, which was ignored for the peak to peak output voltage measurements.

The smart cells operating in Fig. 9 settled to the same switching pattern as the simulated cells in Section VIII.

C. SOC Controller Performance

A second experiment to verify the performance of the SOC controller was also conducted. Each smart cell was connected to a fully charged set of cells, as listed in Table II. However, unlike the previous experiments and simulations, each smart cell started by operating with a duty cycle of 0.5. It became the role of the SOC Controller to correct the mismatch in duty cycles to ensure all three smart cells discharged proportional to their capacity.

During operation, the SOC controller estimates the average string voltage by calculating the difference in levels as described in Section VI. Fig. 10 shows how the cell voltages and duty cycles evolved over time during the experiment.

As shown in Fig. 10, the duty cycles vary quite a bit during operation. This is due to the operation of the SOC controller, attempting to yield accurate voltage information from the string of switching smart cells. Since the controller relies on measuring the difference between levels to measure the average string voltage, there are moments during operation where these levels are non-existent, for example, when all of the duty cycles sum to a positive integer. Therefore, to counteract this possibility, if a cell senses that it has not been able to measure the string voltage for more than 2.5 minutes, it increases or decreases its duty cycle by a fixed amount. This will introduce levels into the voltage measured across L_{sc}, and the cells will be able to measure the average string waveform. This is exactly what is happening from about 75 minutes to 200 minutes in the experimental results of Fig. 10. Cell 001 is modifying its duty cycle to get a better string measurement.

Due to the limited sampling resolution of the analog to digital converter, each cell implements a ± 10 mV dead zone [46] around its reference voltage.

At the end of the experiment, the cells were allowed to rest for 10 minutes, and their voltages were measured. The results are shown in Table III, and they are all within 50 mV of each other. This is a very good result considering there is no communication between any of the smart cells. Furthermore, if the SOC controller was not operating, the string imbalance would have been much greater as shown in Fig. 11, where the smallest capacity cell discharges in around 450 minutes,

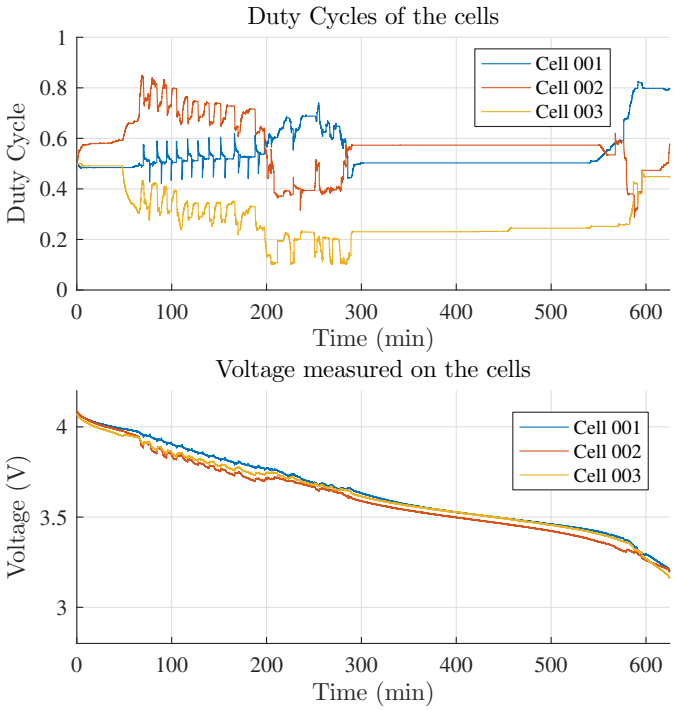


Fig. 10: The evolution of the duty cycles and cell voltages during the SOC controller test. "Steps" in the duty cycle are generated by the SOC controller when an average string voltage measurement cannot be obtained.

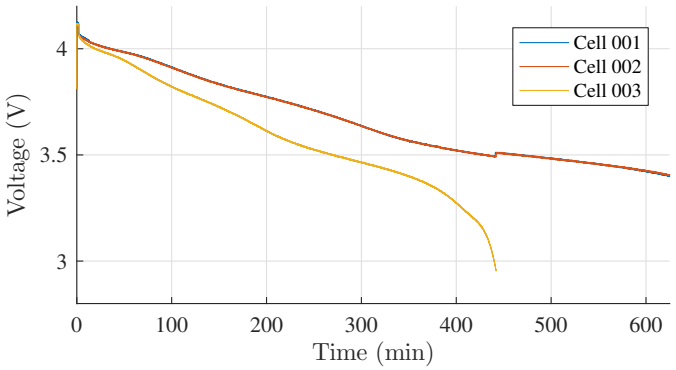


Fig. 11: The evolution of the cell voltages when the SOC controller is disabled, and a constant duty cycle of 0.5 is used by all cells.

clearly limiting the pack performance compared to the SOC controlled case.

TABLE III: Cell voltages at the end of the SOC controller experiment after 10 minutes of rest.

Cell	Voltage (V)
1	3.162
2	3.140
3	3.113

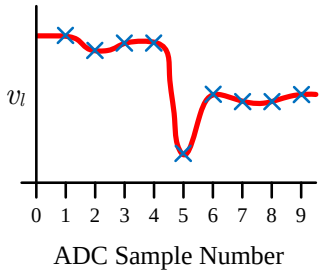


Fig. 12: An example of an ADC sampling a v_l waveform during a switching action with switching noise.

X. Extension to a large number of cells

In theory, the smart cell algorithms scale well with the number of cells, and are limited only by the sampling frequency of the ADC, as briefly mentioned in Section IX. An ADC which can sample quickly will be able to capture all of the salient features of the v_l waveform highlighted in Fig. 2, as required by the algorithm. Alternatively, if the ADC sampling rate is limited, the switching frequency of the smart cells could be decreased so that more samples of the v_l waveform can be captured every switching cycle.

For the system of three smart cells implemented in Section IX, the signal processor had to first identify the switching events by analyzing the output of the captured v_l waveform. The system was able to take 139 samples of v_l during the 20 kHz switching period. Fig. 12 is a drawing of what is recorded by the ADC during a switching event. As shown, there is a relatively constant value of v_l for samples 1 to 4, a cell switches just after sample number 4 with some switching noise as shown by the high value of $|dv_l/dt|$ between samples 4, 5, and 6, and then v_l settles down to its new steady state value for samples 6 to 9. In order to accurately capture the switching events, the signal processor implemented a glitch filter to remove switching noise. The glitch filter ensured that there were no high $|dv_l/dt|$ events for at least 1 sample after an initial high $|dv_l/dt|$ event. Therefore using Fig. 12 as a guide, this would mean that the large $|dv_l/dt|$ event that occurred between samples 4 and 5 would be detected and recorded as a switching event, and the large $|dv_l/dt|$ event between sample 5 and 6 would be ignored.

Accurate cell terminal voltage measurements were achieved by averaging two samples before the switching event, and subtracting the average of the two samples after the switching event, ignoring the two samples around the switching event. Again using Fig. 12 as a guide, the higher voltage level would be calculated as the average of samples 2 and 3, and the lower voltage level would be calculated by averaging samples 6 and 7. Samples 4 and 5, which are around the switching event, are ignored.

In conclusion, to obtain accurate cell terminal voltage measurements, there should be at least 4 samples between each switching event. Therefore, keeping in mind that there are two switching events per cell, the smart cell system of Section IX is theoretically capable of operating with up to $\lfloor 139/4/2 \rfloor = 17$ smart cells in series.

Computationally, the smart cell algorithm also scales well with the number of cells. The most computationally demanding part of the algorithm is the signal processor, depicted in Fig. 6, which scales linearly with the number of ADC samples. The SOC controller needs only to average the terminal voltage measurements from the signal processor, a simple operation which scales linearly with the number of cells. The phase controller calculates the reference angle using (7), a relatively simple operation which also scales linearly with the number of cells.

Finally, as the number of smart cells increase, the voltage across each distributed inductor will decrease, leading to difficulties in sensing voltage levels. The accuracy of the voltage balancing is related to the resolution of the ADC, and the gain of the v_l sensor. To overcome this, smart cells could implement the v_l sensor with a variable gain to ensure that they capture all of the information. Since the gain of this sensor is re-calibrated after every measurement, the variable gain can be implemented in a simple, low cost approach with a resistor array.

XI. Conclusions and Future Work

A completely decentralized battery management system has been introduced based around the concept of a smart cell. The smart cell was built around 1) a phase controller, that synchronized all of the switching actions of the cells to minimize the output voltage ripple, and 2) a SOC controller which adjusted the duty cycle of the local smart cell to synchronize the local cell's voltage with the pack voltage, and thus, its state of charge. This work had particular focus on the phase controller: its design and stability. A system of smart cells was shown to be stable around local minima of (5). A practical battery management system could be built around the theory of smart cells by adding a visual indicator to each cell indicating whether or not it has failed, and implementing a complete BMS at the cell level. In this scenario, a central monitoring function is not required and cells could be easily identified for replacement by a user. If high level control of several cells is desired, a low cost, low power, low bandwidth communication system could be added to provide additional pack benefits.

A novel way of augmenting the role of passive filtering components has also been introduced. Typically, power electronic designs measure the current through inductors and the voltage across capacitors to yield the current and voltage states of a system, respectively. In this work, the voltage across the filtering inductor was measured to yield the switching states, and the average state of charge of the system. Augmenting the role of passives has applications across all areas of power electronics, and could yield new methods of sensing and control. For example, one could measure the voltage across the filtering inductor of a buck or boost converter to yield both the input and output voltages with a single sensor. In another example, this work could be extended to use the voltage across v_l as part of a decentralised MMC controller for grid applications.

As presented, the smart cell concept has been shown to operate at the cell level. However, the same decentralized controller can be employed at higher power levels to break a series string of battery cells into packs instead of individual cells.



Fig. 13: An oscilloscope screen shot of the three smart cells operating with synchronized switching, averaging applied with 8 samples. Channel 2, top green trace, is the voltage across L_{sc} of the first smart cell with a capacity of C_1. Channel 2, middle blue trace, is the output voltage ripple. Channel 3, bottom pink trace, is the current in the smart cell inductors.

Future work on the smart cell will include the implementation of a complete battery management system at the cell level, where the state of health, and state of charge will be managed by the decentralized controller. In particular, the SOC controller will be augmented with a battery model to improve its performance.

Finally, some of the phase synchronization work presented here can be used to create completely decentralized MMC converters. Using a simple modification of multiplying (7) by -1, the smart cells can be designed in synchronize their switching actions to produce sinusoidal output waveforms as depicted in Fig. 13.

Acknowledgment

The authors acknowledge the financial support provided by Newtons4th Ltd. (N4L), the Natural Sciences and Engineering Research Council of Canada (NSERC) and Jesus College Oxford. This work also benefited from equipment funded by the John Fell Oxford University Press (OUP) Research Fund.

References

[1] B. Bose, "Global warming: Energy, environmental pollution, and the impact of power electronics," *Industrial Electronics Magazine, IEEE*, vol. 4, no. 1, pp. 6–17, March 2010.

[2] ——, "Power electronics and motor drives recent progress and perspective," *Industrial Electronics, IEEE Transactions on*, vol. 56, no. 2, pp. 581–588, Feb 2009.

[3] S. Vazquez, S. Lukic, E. Galvan, L. Franquelo, and J. Carrasco, "Energy storage systems for transport and grid applications," *Industrial Electronics, IEEE Transactions on*, vol. 57, no. 12, pp. 3881–3895, Dec 2010.

[4] S. Wilkinson. The grid-connected energy storage market is set to explode, reaching a total of over 40 gw of installations by 2022. IHS Technology. [Online]. Available: https://technology.ihs.com/483008/the-grid-connected-energy-storage-market-is-set-to-explode-reaching-a-total-of-over-40-gw-of-installations-by-2022

[5] H. Chen, T. N. Cong, W. Yang, C. Tan, Y. Li, and Y. Ding, "Progress in electrical energy storage system: A critical review," *Progress in Natural Science*, vol. 19, no. 3, pp. 291 – 312, 2009. [Online]. Available: http://www.sciencedirect.com/science/article/pii/S100200710800381X

[6] D. Andrea, *Battery Management Systems for Large Lithium-Ion Battery Packs*. Artech House Publishers, October 2010.

[7] J. Kimball, B. Kuhn, and P. Krein, "Increased performance of battery packs by active equalization," in *Vehicle Power and Propulsion Conference, 2007. VPPC 2007. IEEE*, Sept 2007, pp. 323–327.

[8] D. Strickland, L. Chittock, D. Stone, M. Foster, and B. Price, "Estimation of transportation battery second life for use in electricity grid systems," *Sustainable Energy, IEEE Transactions on*, vol. 5, no. 3, pp. 795–803, July 2014.

[9] C. Zhou, K. Qian, M. Allan, and W. Zhou, "Modeling of the cost of ev battery wear due to v2g application in power systems," *Energy Conversion, IEEE Transactions on*, vol. 26, no. 4, pp. 1041–1050, Dec 2011.

[10] J. Neubauer and A. Pesaran, "The ability of battery second use strategies to impact plug-in electric vehicle prices and serve utility energy storage applications," *Journal of Power Sources*, vol. 196, no. 23, pp. 10 351 – 10 358, 2011. [Online]. Available: http://www.sciencedirect.com/science/article/pii/S0378775311012377

[11] L. Wen-Chen, J.-H. Yen, F.-H. Shieh, and Y.-M. Liao, "Second use of retired lithium-ion battery packs from electric vehicles: Technological challenges, cost analysis and optimal business model," in *Computer, Consumer and Control (IS3C), 2012 International Symposium on*, June 2012, pp. 381–384.

[12] P. Bennett. (2015, June 22) Nissan to recycle electric vehicle batteries for commercial energy storage products. Clean Energy News. [Online]. Available: http://www.cleanenergynews.co.uk/news/storage/nissan-to-recycle-electric-vehicle-batteries-for-commercial-energy-storage

[13] P. Kelly-Detwiler. (2014, January 29) BMW's i3: A new kind of electric vehicle. Forbes Energy. [Online]. Available: http://www.forbes.com/sites/peterdetwiler/2014/01/29/bmws-i3-a-new-kind-of-electric-vehicle/#53035c3c5996

[14] (2012, November 14) GM, ABB demonstrate chevrolet volt battery reuse unit. General Motors. [Online]. Available: http://media.gm.com/media/us/en/gm/news.detail.html/content/Pages/news/us/en/2012/Nov/electrification/1114_reuse.html

[15] R. A. Leising, M. J. Palazzo, E. S. Takeuchi, and K. J. Takeuchi, "Abuse testing of lithium-ion batteries: Characterization of the overcharge reaction of licoo2/graphite cells," *Journal of The Electrochemical Society*, vol. 148, no. 8, pp. A838–A844, 2001.

[16] L. Lu, X. Han, J. Li, J. Hua, and M. Ouyang, "A review on the key issues for lithium-ion battery management in electric vehicles," *Journal of Power Sources*, vol. 226, no. 0, pp. 272 – 288, 2013. [Online]. Available: http://www.sciencedirect.com/science/article/pii/S0378775312016163

[17] J. Zhang, S. Ci, H. Sharif, and M. Alahmad, "Modeling discharge behavior of multicell battery," *Energy Conversion, IEEE Transactions on*, vol. 25, no. 4, pp. 1133–1141, Dec 2010.

[18] C. Pascual and P. Krein, "Switched capacitor system for automatic series battery equalization," in *Applied Power Electronics Conference and Exposition, 1997. APEC '97 Conference Proceedings 1997., Twelfth Annual*, vol. 2, Feb 1997, pp. 848–854 vol.2.

[19] S. W. Moore and P. J. Schneider, "A review of cell equalization methods for lithium ion and lithium polymer battery systems," SAE Technical Paper, Tech. Rep., 2001.

[20] H. sun Park, C.-E. Kim, C.-H. Kim, G.-W. Moon, and J.-H. Lee, "A modularized charge equalizer for an hev lithium-ion battery string," *Industrial Electronics, IEEE Transactions on*, vol. 56, no. 5, pp. 1464–1476, May 2009.

[21] M. Einhorn, W. Roessler, and J. Fleig, "Improved performance of serially connected li-ion batteries with active cell balancing in electric vehicles," *Vehicular Technology, IEEE Transactions on*, vol. 60, no. 6, pp. 2448–2457, July 2011.

[22] M. Einhorn, W. Guertlschmid, T. Blochberger, R. Kumpusch, R. Permann, F. Conte, C. Kral, and J. Fleig, "A current equalization method for serially connected battery cells using a single power converter for each cell," *Vehicular Technology, IEEE Transactions on*, vol. 60, no. 9, pp. 4227–4237, Nov 2011.

[23] P. Weicker, *A Systems Approach to Lithium-Ion Battery Management*. Artech House Publishers, October 2013.

[24] C. Birkl, D. Frost, A. Bizeray, R. Richardson, and D. Howey, "Modular converter system for low-cost off-grid energy storage using second life li-ion batteries," in *Global Humanitarian Technology Conference (GHTC), 2014 IEEE*, Oct 2014.

[25] H. Qian, J. Zhang, J.-S. Lai, and W. Yu, "A high-efficiency grid-tie battery energy storage system," *Power Electronics, IEEE Transactions on*, vol. 26, no. 3, pp. 886–896, March 2011.

[26] M. Rodriguez, Y. Zhang, and D. Maksimovic, "High-frequency pwm buck converters using gan-on-sic hemts," *Power Electronics, IEEE Transactions on*, vol. 29, no. 5, pp. 2462–2473, May 2014.

[27] D. Reusch, D. Gilham, Y. Su, and F. Lee, "Gallium nitride based 3d integrated non-isolated point of load module," in *Applied Power Electronics Conference and Exposition (APEC), 2012 Twenty-Seventh Annual IEEE*, Feb 2012, pp. 38–45.

[28] T. McDonald and V. President, "Gan based power technology stimulates revolution in conversion electronics," *Electronics in Motion and Conversion*, pp. 2–4, 2009.

[29] J. Millan, P. Godignon, X. Perpina, A. Perez-Tomas, and J. Rebollo, "A survey of wide bandgap power semiconductor devices," *Power Electronics, IEEE Transactions on*, vol. 29, no. 5, pp. 2155–2163, May 2014.

[30] T. Kim, W. Qiao, and L. Qu, "Power electronics-enabled self-x multicell batteries: A design toward smart batteries," *IEEE Transactions on Power Electronics*, vol. 27, no. 11, pp. 4723–4733, Nov 2012.

[31] L. Tan, B. Wu, S. Rivera, and V. Yaramasu, "Comprehensive dc power balance management in high-power three-level dc-dc converter for electric vehicle fast charging," *Power Electronics, IEEE Transactions on*, vol. 31, no. 1, pp. 89–100, Jan 2016.

[32] L. Maharjan, T. Yamagishi, and H. Akagi, "Active-power control of individual converter cells for a battery energy storage system based on a multilevel cascade pwm converter," *Power Electronics, IEEE Transactions on*, vol. 27, no. 3, pp. 1099–1107, March 2012.

[33] K. Cermak and M. Bartl, "Decentralized battery management system," in *Electric Power Engineering (EPE), Proccedings of the 2014 15th International Scientific Conference on*, May 2014, pp. 599–603.

[34] Y. Li and Y. Han, "A module-integrated distributed battery energy storage and management system," *Power Electronics, IEEE Transactions on*, vol. PP, no. 99, pp. 1–1, 2016.

[35] T. Morstyn, M. Momayyezan, B. Hredzak, and V. Agelidis, "Distributed control for state of charge balancing between the modules of a reconfigurable battery energy storage system," *Power Electronics, IEEE Transactions on*, vol. PP, no. 99, pp. 1–1, 2016.

[36] S. Abhinav, G. Binetti, A. Davoudi, and F. Lewis, "Toward consensus-based balancing of smart batteries," in *Applied Power Electronics Conference and Exposition (APEC), 2014 Twenty-Ninth Annual IEEE*, March 2014, pp. 2867–2873.

[37] M. M. U. Rehman, F. Zhang, M. Evzelman, R. Zane, and D. Maksimovic, "Control of a series-input, parallel-output cell balancing system for electric vehicle battery packs," in *2015 IEEE 16th Workshop on Control and Modeling for Power Electronics (COMPEL)*, July 2015, pp. 1–7.

[38] F. Zhang, M. M. U. Rehman, H. Wang, Y. Levron, G. Plett, R. Zane, and D. Maksimovi, "State-of-charge estimation based on microcontroller-implemented sigma-point kalman filter in a modular cell balancing system for lithium-ion battery packs," in *2015 IEEE 16th Workshop on Control and Modeling for Power Electronics (COMPEL)*, July 2015, pp. 1–7.

[39] D. Frost and D. Howey, "Novel mmc control for active balancing and minimum ripple current in series-connected battery strings," in *Power Electronics and Applications (EPE'15 ECCE-Europe), 2015 17th European Conference on*, Sept 2015, pp. 1–10.

[40] A. Lesnicar and R. Marquardt, "An innovative modular multilevel converter topology suitable for a wide power range," in *Power Tech Conference Proceedings, 2003 IEEE Bologna*, vol. 3, June 2003, pp. 6 pp. Vol.3–.

[41] J. Ota, T. Sato, and H. Akagi, "Enhancement of performance, availability, and flexibility of a battery energy storage system based on a modular multilevel cascaded converter (mmcc-ssbc)," *Power Electronics, IEEE Transactions on*, vol. 31, no. 4, pp. 2791–2799, April 2016.

[42] S. S. Choi and H. S. Lim, "Factors that affect cycle-life and possible degradation mechanisms of a li-ion cell based on licoo2," *Journal of Power Sources*, vol. 111, no. 1, pp. 130 – 136, 2002. [Online]. Available: http://www.sciencedirect.com/science/article/pii/S0378775302003051

[43] Y. Kuramoto and H. Araki, "Lecture notes in physics, international symposium on mathematical problems in theoretical physics," 1975.

[44] L. Zhong, C. Zhang, Y. He, and Z. Chen, "A method for the estimation of the battery pack state of charge

based on in-pack cells uniformity analysis," *Applied Energy*, vol. 113, pp. 558 – 564, 2014. [Online]. Available: http://www.sciencedirect.com/science/article/pii/S0306261913006430

[45] *Samsung INR18650-29E Datasheet*, September 2012.

[46] A. Prodic, D. Maksimovic, and R. Erickson, "Dead-zone digital controllers for improved dynamic response of low harmonic rectifiers," *Power Electronics, IEEE Transactions on*, vol. 21, no. 1, pp. 173–181, Jan 2006.



Damien F. Frost received the B.A.Sc. and M.A.Sc. degrees from the University of Toronto, Canada in 2007 and 2009, respectively. Before starting his D.Phil (PhD) degree in the Energy and Power Group, Department of Engineering Science, University of Oxford, Oxford, U.K. in 2013, he worked in the solar industry as a co-founder and power electronics designer at ARDA Power. He is currently working towards his D.Phil at Oxford, where his research is focused on the application of power electronics and control theory to battery management systems.



David A. Howey (M'10) received the B.A. and M.Eng. degrees from Cambridge University, Cambridge, U.K., in 2002 and the Ph.D. degree from Imperial College London, London, U.K., in 2010. He is currently an Associate Professor with the Energy and Power Group, Department of Engineering Science, University of Oxford, Oxford, U.K. His research is focused primarily on energy storage systems, including projects on model-based battery management, degradation, thermal management, and energy management for grid storage.